Desalination and Water Treatment
www.deswater.com

doi: 10.5004/dwt.2022.28854

274 (2022) 18–29
October

Hydrophilic polysulfone ultrafiltration membrane incorporated with reduced graphene oxide modified $ZnFe_2O_4$: application in the separation of simulated natural organic wastewater

Wensong Duan*, Yongzheng Lian, Ting Li, Wenjie Wang, Yue Wang

Anhui Normal University School of Ecology and Environment, Anhui Wuhu, 241000, China, emails: dws7911@163.com (W.S. Duan), 2827127239@qq.com (Y.Z. Lian), 1059070376@qq.com (T. Li), 2900316619@qq.com (W.J. Wang), 2396312932@qq.com (Y. Wang)

Received 9 May 2022; Accepted 17 August 2022

ABSTRACT

A novel polysulfone ultrafiltration membrane for wastewater treatment was fabricated using the non-solvent induced phase inversion (NIPS) technique. The modifier was zinc ferrate-reduced graphene oxide ($ZnFe_2O_4$-rGO) nanocomposite, which was prepared by sol–gel. The optimum concentration of addiction was found to be 0.1 wt.%, where the hydrophilicity and permeability of the membrane were significantly improved. On this condition, the membrane had a water contact angle of 63.5° and pure water permeance of 517.06 LMH·bar^{-1}. The membrane resistance was 1.17×10^{12} m^{-1}. Moreover, the strength increased by 85.28 cN and the elongation increased by 10.22% with the addition of particles. The results of interception and anti-contamination analysis of three natural organic matters and secondary effluent organic compounds by composite membrane showed that the optimal loading capacity was 0.04 wt.%, and the interception rates of bovine serum albumin, humic acid, and sodium alginate were 95.03%, 73.89%, and 94.50%. After three cycles, the rejection rates were kept 94.50%, 94.72% and 94.87%. The maximum flux recovery was 97.92%, 98.15%, and 93.95%. Meanwhile, the irreversible pollution decreased to 19.80%, 19.98%, and 15.98%. In brief, a small amount of $ZnFe_2O_4$-rGO NPs can be used to successfully modify the hydrophilicity, permeability, and rigidity cantifouling ability of the membrane.

Keywords: $ZnFe_2O_4$-rGO; Polysulfone; Ultrafiltration membrane; Antifouling; Hydrophilicity

1. Introduction

As a thermoplastic polymer material, polysulfone (PSF) is extensively used for the fabrication of ultrafiltration membranes due to its strong chemical stability, good acid and alkali resistance, low cost and harmless properties [1,2]. However, its hydrophobicity often leads to increased membrane resistance, increased membrane pollution, and higher operating costs. Thus, the modification of polysulfone membrane to enhance its hydrophilicity, alleviate membrane pollution and prolong membrane life has attracted the attention of researchers. The composite of polymers and nanomaterials can concentrate the advantages of these materials to form a composite material with unique functions. The modification methods of polysulfone membrane mainly include blending modification and surface modification. Blending modification refers to the preparation of a composite membrane by uniformly mixing inorganic nanomaterials and casting solution, which aims to organically combine particle characteristics with membrane interception and separation to improve the comprehensive performance of the membrane [3–5]. To date, numerous

* Corresponding author.

nanomaterials such as titanium dioxide (TiO_2) [6], graphene oxide (GO) [4], silicon dioxide (SiO_2) [7], dopamine (PDA) [8] are used to fabricate modified ultrafiltration (UF) membranes, which to improve the hydrophilicity, antifouling and antibacterial properties of the membrane. Since polymers with lower surface energy preferentially migrate to the surface in polymer blends [9], many studies have synthesized surface-modified macromolecules to improve the properties [10], hydrophilic/hydrophobic [11], chargeability [12] and anti-fouling properties [13] of membranes.

With the development and application of nanomaterials, studies on photocatalytic degradation of organic pollutants, photohydrolytic hydrogen production, and photochemical synthesis are emerging increasingly [14]. Ferrite has attracted extensive attention in recent years due to its excellent magnetic and photocatalytic properties. Tahereh et al. [15] used zinc ferrite-silicon dioxide ($ZnFe_2O_4$-SiO_2) as a new adsorbent to effectively remove Congo red in the water. Mady et al. [16] synthesized silver-zinc ferrite-reduced graphene oxide (Ag-$ZnFe_2O_4$-rGO) by microwave assisted synthesis, which effectively degraded methylene blue (MB), Rhodamine B (RhB) and methyl orange (MO) in water. LAN Ranran et al. [17] prepared polyvinylidene fluoride (PVDF) composite membrane by doping $BaFe_{12}O_{19}$ with barium ferrite, which greatly improved the dielectric and thermodynamic properties of the membrane material. Kallem et al. [18] used PDA-$ZnFe_2O_4$ to prepare polyethersulfone (PES) ultrafiltration membrane for wastewater treatment. The humic acid (HA) removal and oil-water separation ability of the membrane were improved. In general, polymers are immiscible in the absence of specific interactions between them [19]. Therefore, too much ferrite added to PSF will lead to agglomeration. Due to its large specific surface area, good water dispersion and high adsorption capacity, GO can not only modify the polymer membrane but also serve as the dispersion medium of other nanoparticles. However, the high cost restricts its application in water purification [20–23]. The doping nanoparticles can adjust the interlayer spacing of GO, and the lamella can also be used as the dispersion carrier of particles. Moreover, the surface of GO contains a large number of active groups, such as hydroxyl (–OH), carbonyl (C=O), carboxyl (–COOH), ester (–COO–), so GO has good compatibility with PSF. Therefore, GO/$ZnFe_2O_4$ composites can improve the poor compatibility and agglomeration of ferrite and PSF While the two-dimensional layered rGO two-dimensional lamella has a larger specific surface area, which is conducive to the dispersion of semiconductor nanomaterials, and excellent electrical conductivity. Wu et al. [24] showed that $ZnFe_2O_4$-rGO composite material significantly enhanced the visible light (550–800 nm) absorption capacity of $ZnFe_2O_4$. The synthesized material improved the efficiency of photocatalytic degradation of dyes. Li et al. [25] studied the degradation effect of graphene-loaded $ZnFe_2O_4$ composite material on dyes. The result showed that magnetic $ZnFe_2O_4$-GO could rapidly catalyze the decolorization of Congo red under simulated sunlight irradiation, with a removal rate of 92% and stable photocatalytic activity.

The purpose of this study is to fabricate $ZnFe_2O_4$-rGO/PSF with improved permeability, separation, and antifouling properties via non-solvent induced phase inversion using nanocomposites of $ZnFe_2O_4$-rGO as an additive in the casting solution. The effects of different amounts of particles on the microstructure and properties of the membrane were studied. Bovine serum protein, humic acid and sodium alginate were used to simulate three natural organic matters (NOMs) to explore the resistance of the membrane to contamination. The effect of modified membrane on the removal of organic compounds in secondary effluent under different light conditions was also revealed. The results provide a research idea and theoretical basis for the application of ferrite-modified polysulfone membrane in water treatment.

2. Experimental details

2.1. Materials

Polysulfone (PSF, P1700) was purchased from BASF (Germany). Polyvinylpyrrolidone (PVP, ≥95%), N,N-dimethylacetamide (DMAc, 99.5%), zinc nitrate, ascorbic acid, urea were purchased from National Reagent (China). Ferric nitrate, bovine serum albumin (BSA), humic acid (HA), and sodium alginate (SA) were supplied by McLean company (China). GO suspension (2 mg mL^{-1}) was got from SuZhou TanFeng company (China). Ultrafilter cup SCM-300 was purchased from Snapp company (China); Wet film preparator SZQ-400 (200 μm) was supplied by Shanghai Pushen company (China); Experimental device is shown in Fig. 1.

2.2. $ZnFe_2O_4$-rGO synthesis and functionalization

It was prepared by the sol-gel method. According to the mole ratio of 1:2 says take a suitable amount of zinc nitrate and ferric nitrate is dissolved in deionized water to get A solution. Then take graphene oxide suspension after ultrasonic B. A, B mixture stirring will get the solution C. Adding the suitable amount of ascorbic acid and urea completely dissolved after growing until clear water residue after getting the precursor gel in A vacuum oven to 80°C drying 12 h. Calcination at high temperature in a muffle furnace at 500°C and grinding after cooling to obtain $ZnFe_2O_4$-rGO [18].

2.3. Membranes fabrication

A proper amount of polysulfone (PSF), polyvinylpyrrolidone (PVP), $ZnFe_2O_4$-rGO powder, and N,N-dimethylacetamide (DMAc) were mixed in a 250 mL bethel, and mechanically stirred at 65°C until a uniform and stable casting solution was formed. Then, the solution was stood in a vacuum oven at 60°C for 12 h. Pour the defoaming liquid onto the clean glass plate, and scrape the uniform liquid film with a 200 μm scraper at a uniform speed. After curing for a certain time, put it into the pure water coagulation bath until the film is completely separated, and transfer it to DI for use. The film making series are shown in Table 1.

2.4. Characterization of $ZnFe_2O_4$-rGO particles

The crystallization structure of the prepared particle was obtained by X-ray diffraction (XRD) model D8 FOCUS diffractometer with Cu Ka radiation. To investigate the

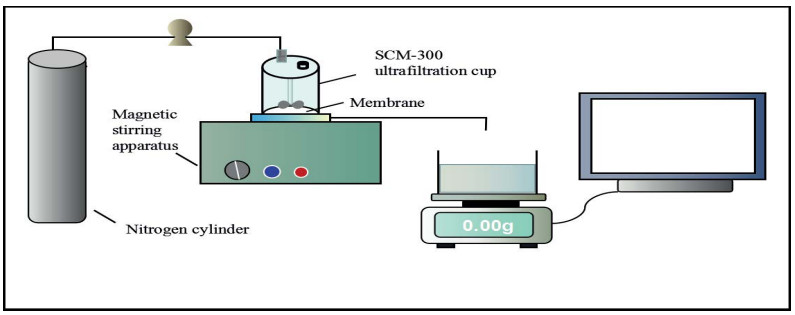

Fig. 1. Diagram of laboratory dead-end filter device.

Table 1
$ZnFe_2O_4$-rGO compositions in the prepared membranes

Membranes	PSF (wt.%)	PVP (wt.%)	DMAc (wt.%)	$ZnFe_2O_4$-rGO (wt.%)
P0	15	2	83.00	0.00
P1	15	2	82.98	0.02
P2	15	2	82.96	0.04
P3	15	2	82.90	0.10
P4	14	2	82.80	0.20

surface morphology of the $ZnFe_2O_4$-rGO, scanning electron microscopy (SEM) S-4800 (Hitachi, Japan) was used.

2.5. Surface characterization of the membranes

For further study of the influence of $ZnFe_2O_4$-rGO usage on the polysulfone matrix, the functional groups of the blending matrix were characterized by FT-IR (Avatar-360, Nicolet, USA) spectrometer in the range of 500–4,000 cm^{-1}. To follow the surface and cross-section morphology of the membranes, a scanning electron microscope (SEM, S-4800, Hitachi, Japan) was utilized. The roughness of the membrane surface was determined by atomic force microscopy (AFM, Bruker Dimension Icon). The hydrophilicity of the membranes was identified by water contact angle using DSA30 (Germany Kruss). The mechanical strength of the composite film was evaluated by AGS-H (Shimadzu, Japan), the clamping distance is 20 mm and the speed of stretching is 10 mm min^{-1}.

2.6. Permeability and rejection determination

The permeation, rejection, and antifouling properties of the membranes were studied using a homemade dead-end filter (SCM300) with an effective area of 3.32 × 10^{-3} m^2. Pure water flux (J_w, LMH·bar^{-1}), pollutants rejection (R, %), membrane resistance and porosity were determined by the following equations:

$$J_w = \frac{V}{A \times \Delta T} \tag{1}$$

$$R = \left(1 - \frac{C_p}{C_f}\right) \times 100\% \tag{2}$$

$$p = \frac{\left(W_w - W_d\right)/\rho_w}{\left(W_w - W_d\right)/\rho_w + W_2/\rho_P} \times 100\% \tag{3}$$

$$R_m = \frac{\Delta P}{\mu \times J_w} \tag{4}$$

where V (L) is the volume of permeate, A (cm^2) is the effective membrane area, ΔT (h) is the sampling time, W_w and W_d are wet and dry membrane weight, respectively. ρ_w is the density of water at 23°C (0.998 g cm^{-3}) and ρ_p is the density of polysulfone (1.24 g cm^{-3}). ΔP (MPa) is the operational pressure and μ is the viscosity of pure water at 23°C (9.3 × 10^{-4} Pa·s). R is named as pollutants rejection (%), C_f and C_p are the pollutant concentration in the feed and permeate, respectively.

2.7. Dynamic fouling experiments

BSA, HA, and SA were used to simulate the protein, humus, and alginate pollutants in natural organic matter, the antifouling performance of bare and $ZnFe_2O_4$-rGO/PSF membranes was evaluated by parameters that were named flux recovery ratio (FRR), reversible fouling ratio (Dr) and irreversible fouling ratio (Dir) by the following process. The primary pure water flux (J_1) was recorded after 30 min filtration test. Then pollutant solution in the concentration of 1,000 mg L^{-1} was replaced and filtered for 30 min at 1.5 bar, the foulant flux (J_p) was recorded. After filtration, distilled water was used to wash fouled membranes for 30 min. Finally, the steady water flux was recorded (J_2) as the same as the first filtration after washing. The following equations were used:

$$\text{FRR} = \frac{J_2}{J_1} \times 100\% \tag{5}$$

$$D_{\mathrm{Rr}} = \left(\frac{J_2 - J_p}{J_1}\right) \times 100\% \quad (6)$$

$$D_{\mathrm{Rir}} = \left(\frac{J_1 - J_2}{J_1}\right) \times 100\% \quad (7)$$

The following cycles were repeated in the same steps as cycle 1, the FRR was recorded for each cycle. Each concentration of foulants were estimated by UV-VIS spectrophotometer (UV752, Shanghai). All experiments were studied at room temperature.

2.8. Cycle performance

The prepared membrane was tested for three pollution cycles of 210 min, and the flux recovery and rejection changes under each cycle were explored to explore the recycling usability of the membrane.

3. Results and discussion

3.1. Morphology characterization of the particle

The structure of the $ZnFe_2O_4$-rGO particle photographed by SEM is shown in Fig. 2, and zinc ferrite particle is clearly attached to the GO layer. The particle size analysis of any 150 particles in the figure by Image *J* shows that composite particles are distributed in the range of 20~100 nm with an average particle size of 51.87 nm.

The X-ray diffraction spectrum for the $ZnFe_2O_4$-rGO nanohybrid is shown in Fig. 3, which illustrated the existence of rGO loaded with $ZnFe_2O_4$. According to previous studies, GO has a strong characteristic peak at 10.91° belonging to the (001) crystal plane of GO. The characteristic peak of reduced graphene oxide (rGO) is around 25° [17]. The characteristic diffraction peaks at 18.03°, 29.98°, 36.58°, 36.80°, 42.92°, 53.26°, 56.68° and 62.12° are respectively attributed to (111), (220), (311), (222), (400), (422), (511) and (400) crystal planes of $ZnFe_2O_4$. The special diffraction peaks at 30.90°, 36.08°, 45.74° and 65.22° are attributed to the (100), (101), (102) and (112) crystal planes of ZnO, respectively. In addition, the weak diffraction peak at 41.94° corresponds to the (200) crystal plane of FeO [18,19], indicating that ZR was partially reduced and FeO by-products were generated under alkaline preparation conditions.

3.2. Membrane characterization

3.2.1. FT-IR

FT-IR spectra of the bare and $ZnFe_2O_4$-rGO/PSF composite membranes are presented in Fig. 4. The absorption peaks of P0 and P2–P4 at 411 and 558 cm^{-1} were compared and attributed to the stretching vibration of Fe–O and Zn–O bonds in $ZnFe_2O_4$. In addition, a wide peak at 3,472 cm^{-1} can be attributed to the O–H stretching vibration of GO and water. The three absorption peaks at 1,480; 1,150 and 1,590 cm^{-1} were caused by C–OH, C–O, and C=O vibration respectively, and the weak absorption peak at 1,673 cm^{-1} was caused by stretching vibration of the C=C conjugate skeleton. The absorption peak at 1,240 cm^{-1} is attributed to the sulfone group (–SO_2–) in the polysulfone membrane matrix [26]. The characteristic peaks at 411 and 588 cm^{-1} were enhanced with the increase of adding amount, indicating that the blending film was successfully prepared and the addition amount of $ZnFe_2O_4$-rGO particles affected the element distribution on the film surface.

3.2.2. Morphology (SEM and AFM)

The SEM morphology of the surfaces and corresponding sections of P0, P2, P3, and P4 are shown in Fig. 5. All prepared membranes have a common asymmetric structure. From (a), it can be seen that the original PSF film before modification is rough and dense, with sparse membrane pores and a small pore diameter. The clear dense surface layer and finger-like and spongy curved sub-surface structure can be seen in the section at 500 times. With the addition of nanoparticles, the hydrophilic effect accelerates the mass transfer rate, and the expansion of pore

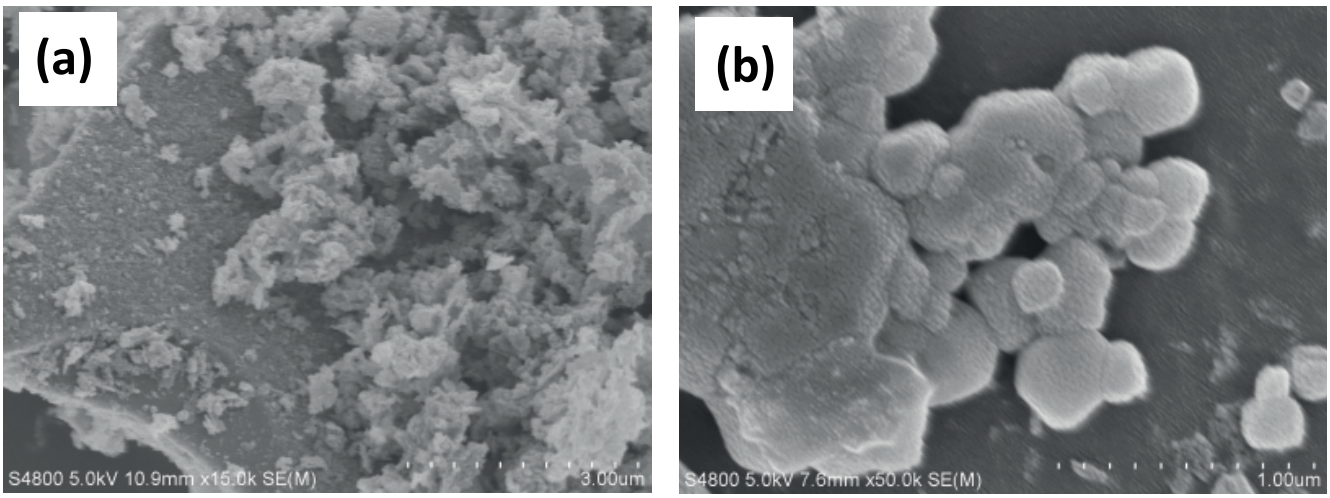

Fig. 2. SEM images of $ZnFe_2O_4$-rGO particle.

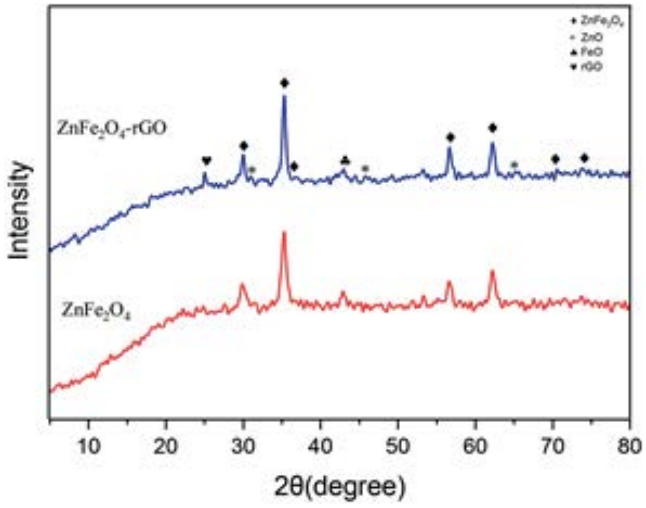

Fig. 3. XRD patterns of $ZnFe_2O_4$ and $ZnFe_2O_4$-rGO particles.

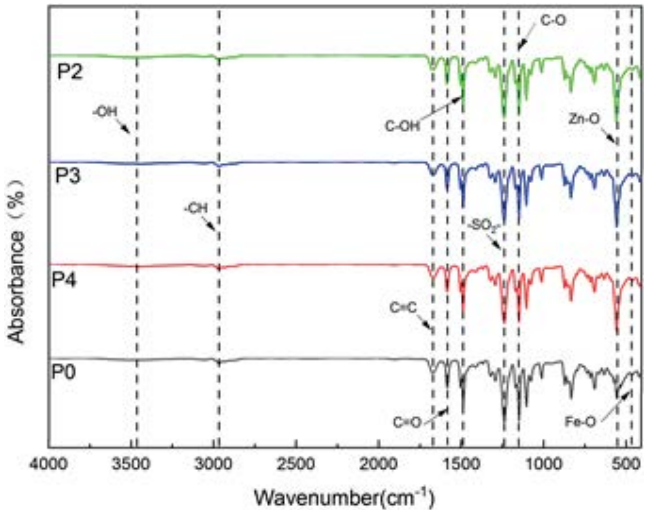

Fig. 4. Infrared spectrum of ZR modified polysulfone film.

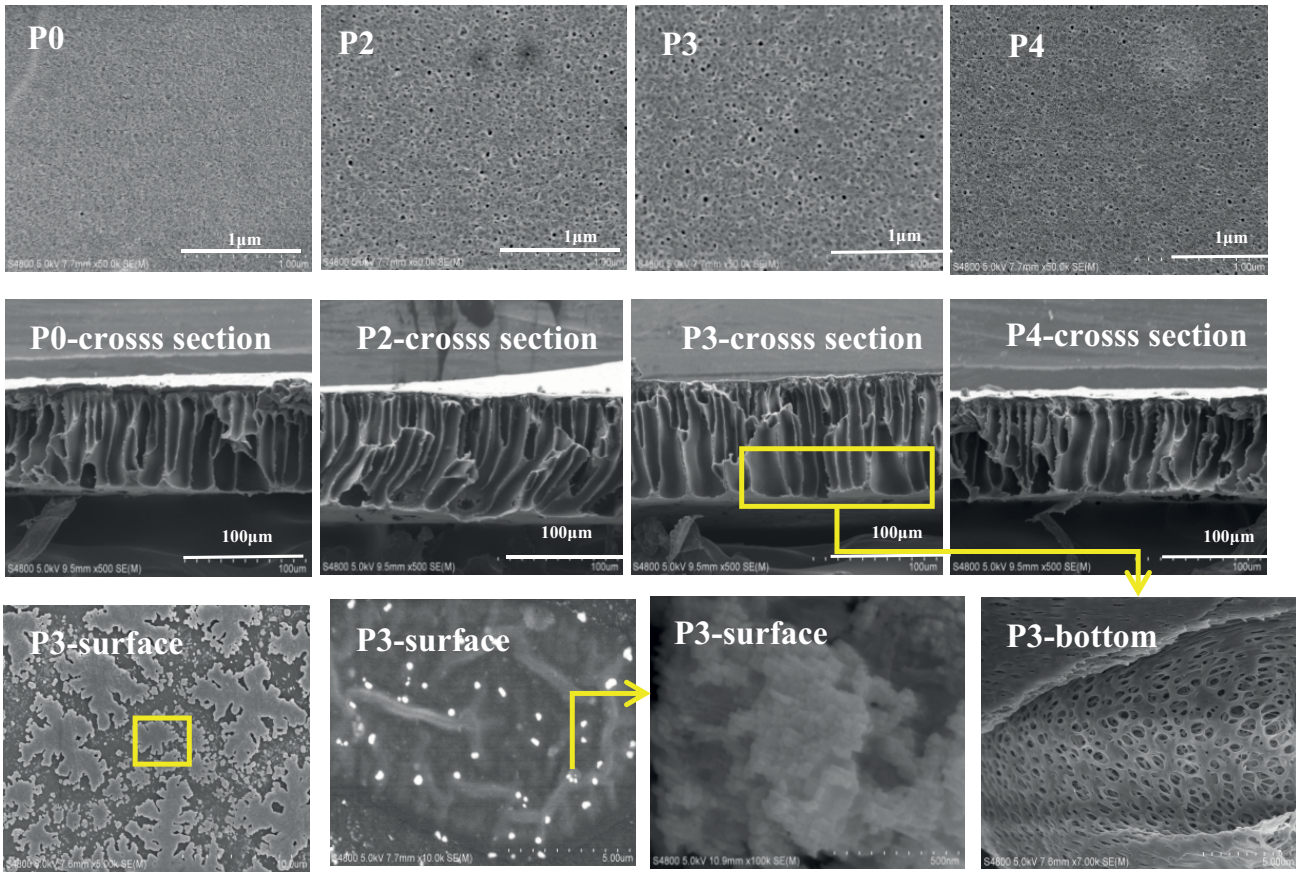

Fig. 5. SEM images of surface and cross-section of ultrafiltration membrane.

channels makes the formation of finger-like large pores more uniform and regular, the connection between pores denser, and the number of pores increased significantly.

Fig. 6 represents the top surface 2D AFM images, which play an important role in analyzing the tendency of fouling. The roughness parameters were investigated mean roughness (R_a) and root mean square (R_q) of the tested membranes are listed in Table 2, which is depicted from AFM results. Clearly, R_a and R_q were found to decrease after the low addition of nanoparticles, which indicates that modified membranes were smoother than the neat ones. The reduction in roughness was due to hydrophilic

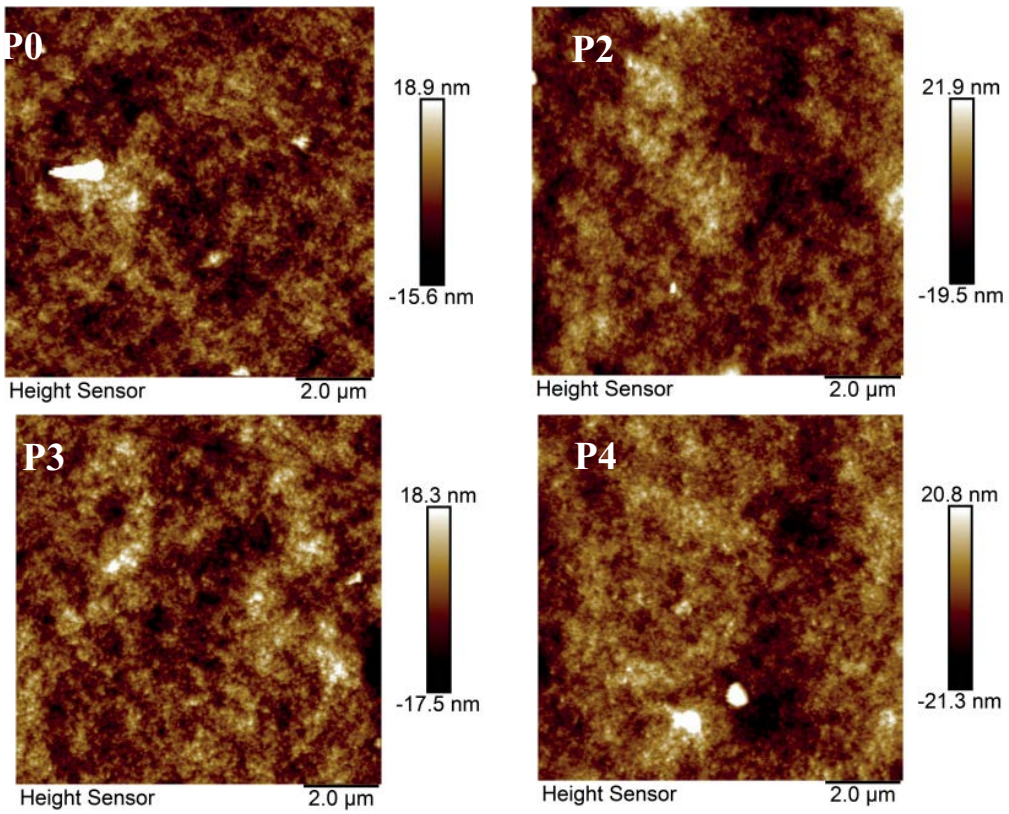

Fig. 6. Surface roughness of ultrafiltration membrane.

groups interacting on the surface of the film to form a hydration layer. When the loading capacity increased to 0.1 wt.%, the roughness increased slightly, indicating that the particle concentration was easy to agglomerate on the film surface, and the morphology of the peak valley bump on the film surface increased, and the roughness increased. The average pore size of all mixed membranes is larger than P0, which was reasonable due to the hydrophilic nanoparticles into PSF casting solutions accelerated the exchange rate between solvent and non-solvent during the phase inversion method, resulting in the porous structure of the mixed matrix membranes. While after the addition of 0.1 wt.%, the viscosity of the casting solution and its increasing trend decrease the average pore size. Last but not least, these data may display that prepared membranes with larger roughness are more prone to higher fouling propensity due to the accumulation of pollutants in the surface valleys, which decreases the fouling resistance capability of the membrane.

Table 2
Roughness and mean pore size of modified membranes

Membranes	R_a	R_q	Mean pore size
P0	5.41 ± 0.33	6.06 ± 0.92	13.86 ± 1.37
P2	4.01 ± 0.31	5.62 ± 0.07	17.74 ± 3.21
P3	3.94 ± 0.19	5.22 ± 0.12	18.46 ± 4.47
P4	4.74 ± 0.32	5.98 ± 0.55	17.83 ± 3.85

3.2.3. Hydrophilicity

Surface hydrophilicity is a significant indicator of the ultrafiltration membrane that has an impact on the separation and permeation. The parameter of water contact angle was studied and is illustrated in Fig. 7. It can be seen that the angle of the original film is 88.2°, which means the hydrophilicity of the bare membrane is poor. While it decreases to 63.5° after adding 0.1 wt.% particles. Obviously, the hydrophilicity of the modified polysulfone membrane is improved. This reduction may be ascribed to the interaction of hydroxyl, carboxyl, epoxy, and other hydrophilic groups containing oxygen groups on particles. Hydrogen bonds are formed between particles and water molecules, which reduces the surface tension between water molecules and the membrane, thus reducing the contact Angle and enhancing the dependence of the membrane on water.

3.2.4. Mechanical strength

Fig. 8 shows the breaking strength and elongation of the fabricated membranes. It is well known that polysulfone membrane is often damaged under stress due to its insufficient mechanical strength under certain pressure. The strength and elongation improved 85.28 cN and 10.22% after increasing $ZnFe_2O_4$-rGO particles. It may be ascribed to the fact that hydrogen bonding between the nano-additive

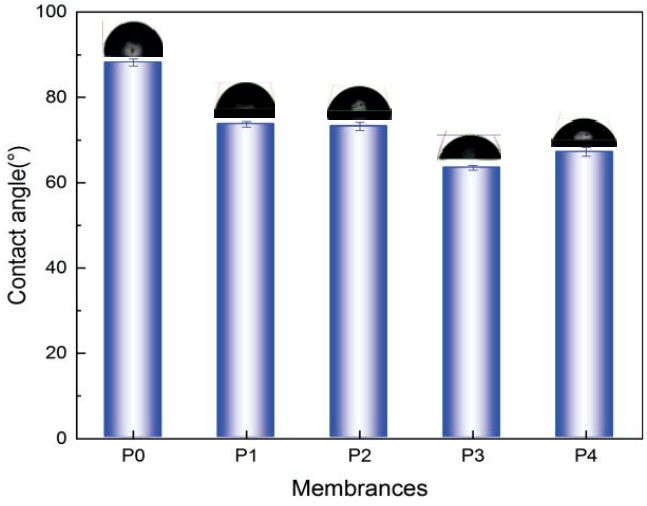

Fig. 7. Water contact angle before and after modification of ultrafiltration membrane.

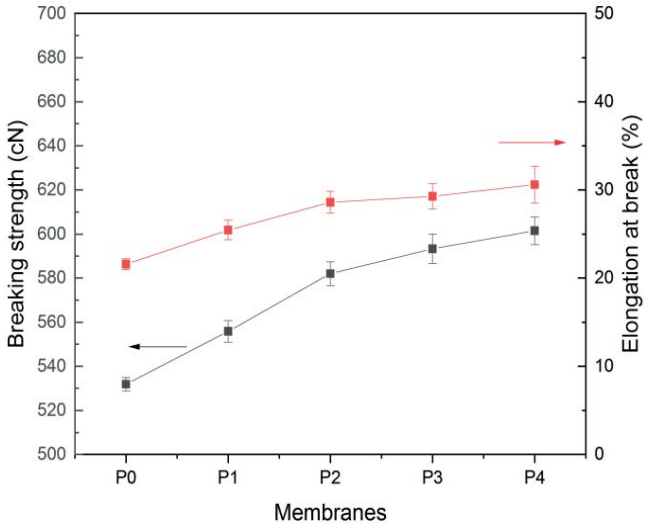

Fig. 8. Mechanical strength of ultrafiltration membrane.

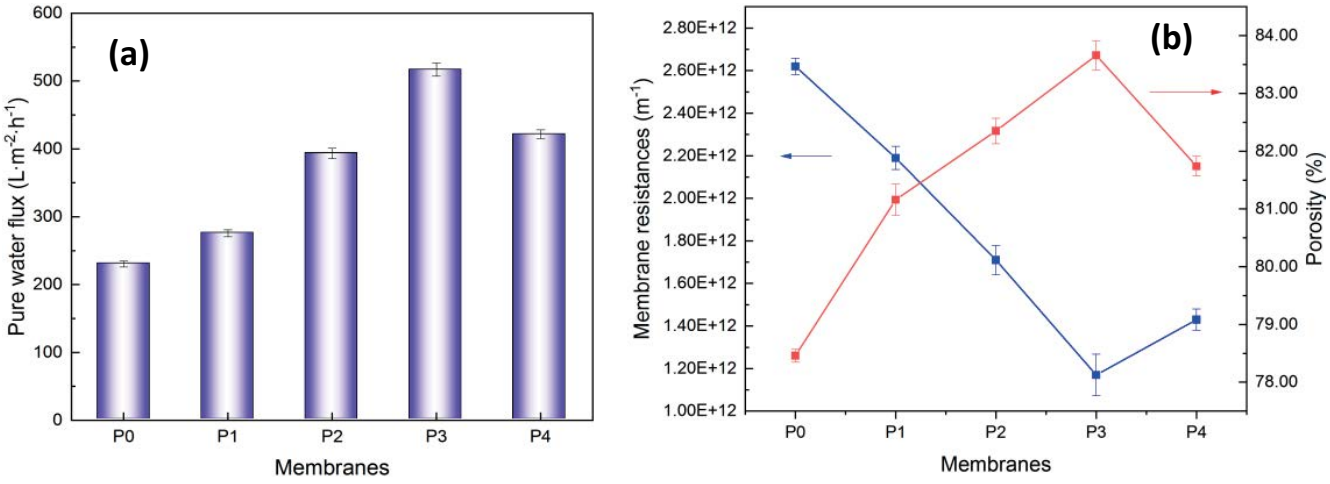

Fig. 9. Pure water flux, porosity and resistance of ultrafiltration membrane (a) pure water flux and (b) porosity and resistance.

and the polymer matrix, covalently binding to the polymer chain. Nanoparticles act as connectors to the polymer chain, thereby increasing the rigidity of the polymer.

3.3. Membrane properties

3.3.1. Permeability, porosity and resistance

Overall pure water flux, porosity and resistance of the fabricated membranes are calculated and shown in Fig. 9. The flux of the pristine membrane was 230.24 ± 4.35 LMH·bar^{-1}. The results displayed that by the addition of 0.1 wt.% of $ZnFe_2O_4$-rGO to the blending matrix, the value of flux was significantly improved to 517.06 ± 9.75 LMH·bar^{-1}. While, with further increase of the particles, it exhibited obvious decreases to 421.54 ± 6.51 LMH·bar^{-1}. This fact attributed that the embedding of nanofiller changes the hydrophilicity of the casting solution which accelerates the separation of solvent and non-solvent during the film-forming process. Nevertheless, excessive loadings are likely to cause the enhancement of solution viscosity and agglomeration of the particles which resulting the pores of the membrane being blocked. With the addition of particle amount, the porosity increased from 78.46% to 83.66%, and the membrane resistance decreased from 2.62 × 10^{12} m^{-1} to 1.17 × 10^{12} m^{-1}. It was attributed to the fact that the hydrophilic groups in the particles accelerate the material exchange rate in the phase transformation process, which promotes the formation of pores. In summary, the above results illustrated that the hydrophilic additives in the membrane matrix can effectively reduce the interfacial resistance and remarkably improve the permeability of the membrane.

3.3.2. Antifouling ability of the membranes

As shown in Fig. 10, the best rejection rates of BSA, HA, and SA were 95.03%, 73.89% and 94.50%, respectively. The reason for the improvement in rejection could be ascribed to the narrow interlamellar nano-channels and nano-scale

membrane pores of rGO in $ZnFe_2O_4$-rGO particles to separate pollutants. It makes it easier for water molecules to pass through while trapping larger contaminants, creating what is known as the dimensional exclusion effect. The interception order of three types of pollutants was similar, SA > BSA > HA. SA is easy to form a dense polluted film on the film surface, and the hydrophilic hydrated layer of the modified film can make the structure of the SA contaminated layer looser. HA is considered to be an important hydrophobic membrane fouling component, which often contaminates the gel layer by forming a network through internal crosslinking [27]. In addition, it was possible that Zn ions contained in particles may lead to the formation of HA-Zn consortium, which neutralizes the negative charge on HA molecules, reduce the tensile degree of HA molecules and make them smaller [28,29], due to the low rejection of HA.

The reversible pollution Dr and irreversible pollution Dir after the initial cycle of the three pollutants are estimated in Fig. 11a–c for BSA, HA and SA, respectively.

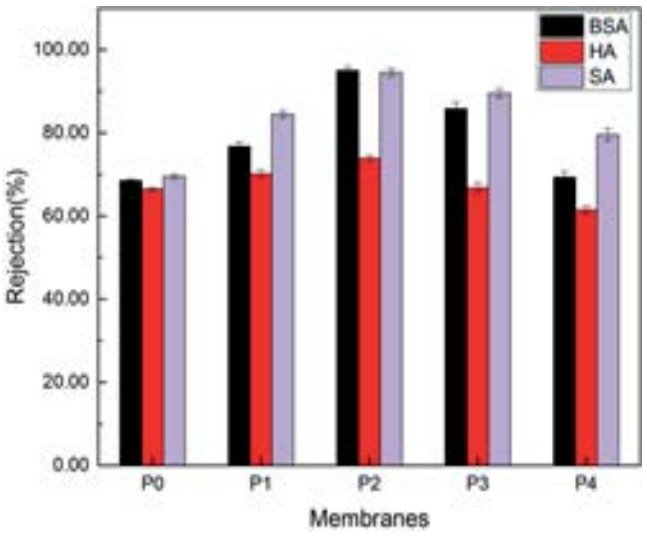

Fig. 10. Rejection of modified films on BSA, HA and SA.

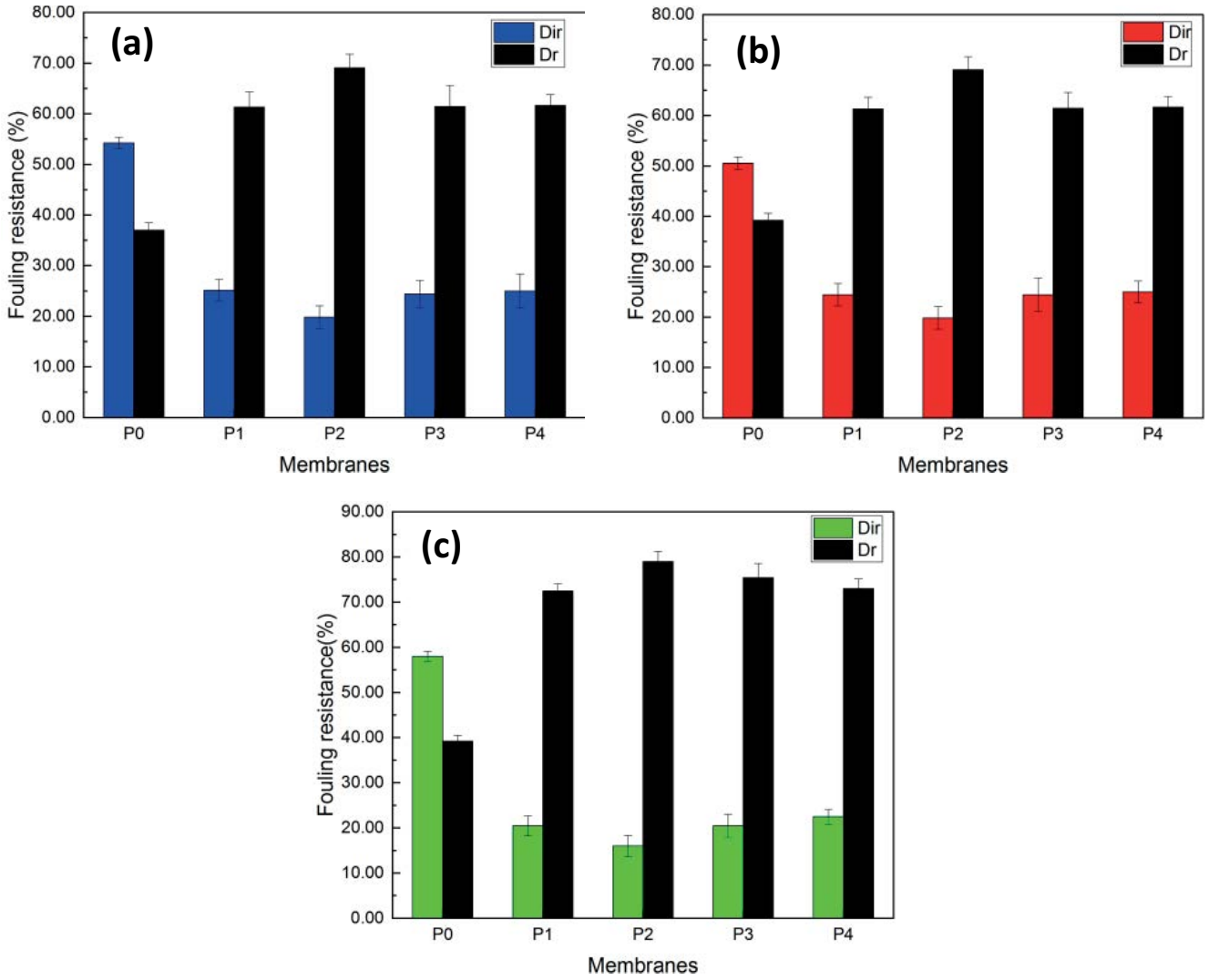

Fig. 11. Fouling resistance of modified films on (a) BSA, (b) HA and (c) SA.

Compared with the original PSF, all $ZnFe_2O_4$-rGO composite films showed a lower irreversible fouling ratio (Dir) and a higher reversible ratio (Dr). The reversible contamination (Dr) of BSA, HA and SA were 36.96%, 39.23% and 39.18%, respectively, and increased to 69.08%, 69.99% and 78.99%, respectively, with the addition of 0.04 wt.% $ZnFe_2O_4$-rGO particles. The irreversible pollution decreased from 54.24%, 50.53% and 57.98% to 19.80%, 19.98% and 15.98%, respectively. Compared with P3 and P4, it is found that the irreversible pollution Dir increases, which is due to the high content of particle additives, agglomeration of particles resulting in larger roughness of the membrane surface, and the increasing gullies on the membrane surface resulting in more binding sites of pollutants, which ultimately leads to the aggravation of the pollution tendency of the membrane. Compared with P2 and P3, it was found that the membrane with the best flux and hydrophilicity did not show the best anti-pollution effect. The study showed that the anti-pollution effect of the membrane was affected by multiple factors, including membrane structure, pore size distribution, and membrane surface charge, etc. High surface roughness, large aperture, wide aperture distribution and high flux lead to high pollution [30]. Composite membranes are more resistant to protein and organic contamination.

3.3.3. Cycle performance

Fig. 12 gives us comprehensive information regarding the dramatic reduction in the permeate flux when pure water was replaced by the fouling agent and then the stable flux was achieved. Stable cycling performance is particularly important in the use of ultrafiltration membranes. When the pollutant solution is filtered, the flux drops rapidly to a lower level and continues to decline, which is caused by the blockage of membrane holes caused by the adsorption of pollutant solution on the membrane surface and membrane

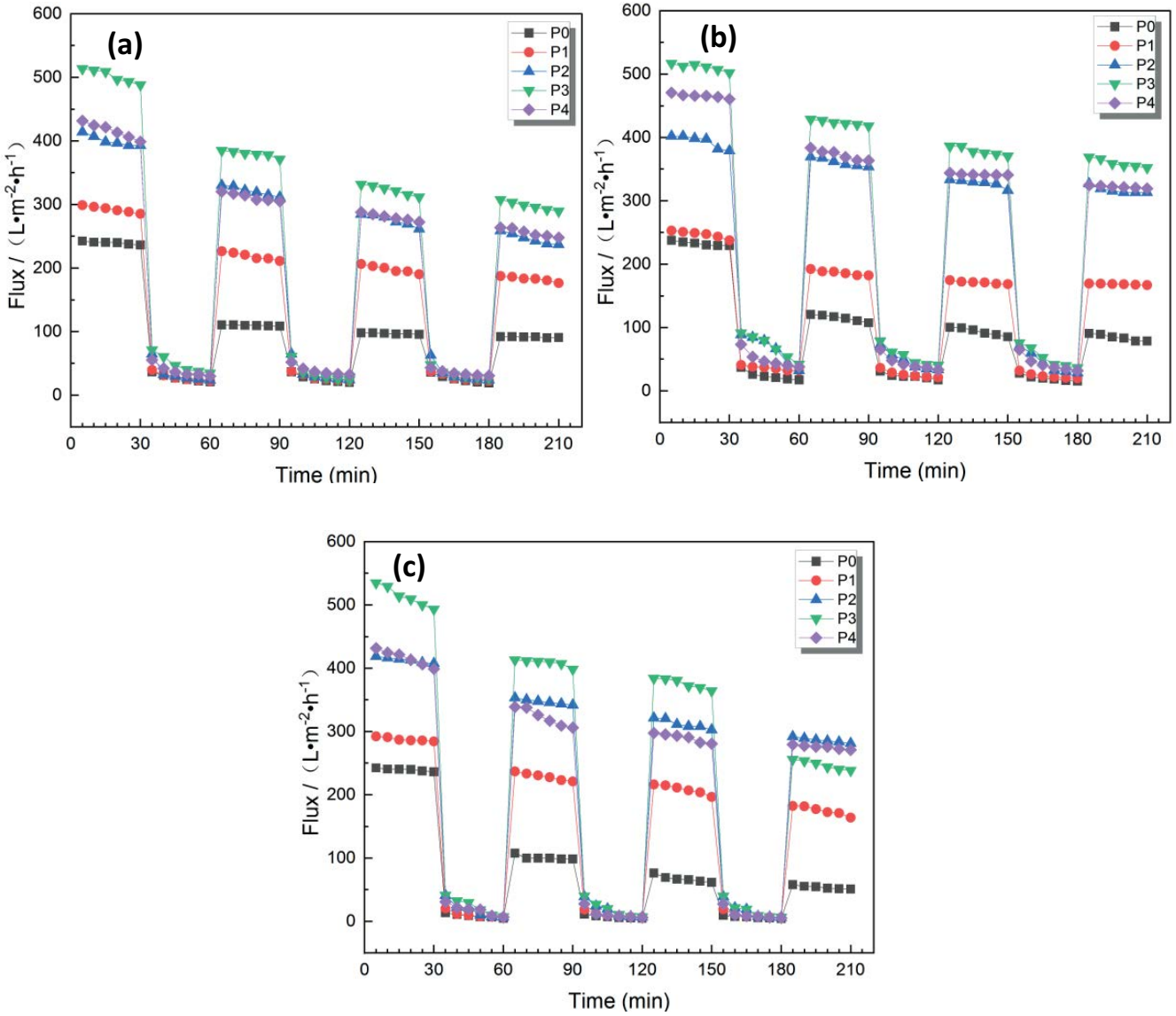

Fig. 12. Cycling properties of polysulfone membranes modified with different ZR mass fractions: (a) BSA, (b) HA and (c) SA.

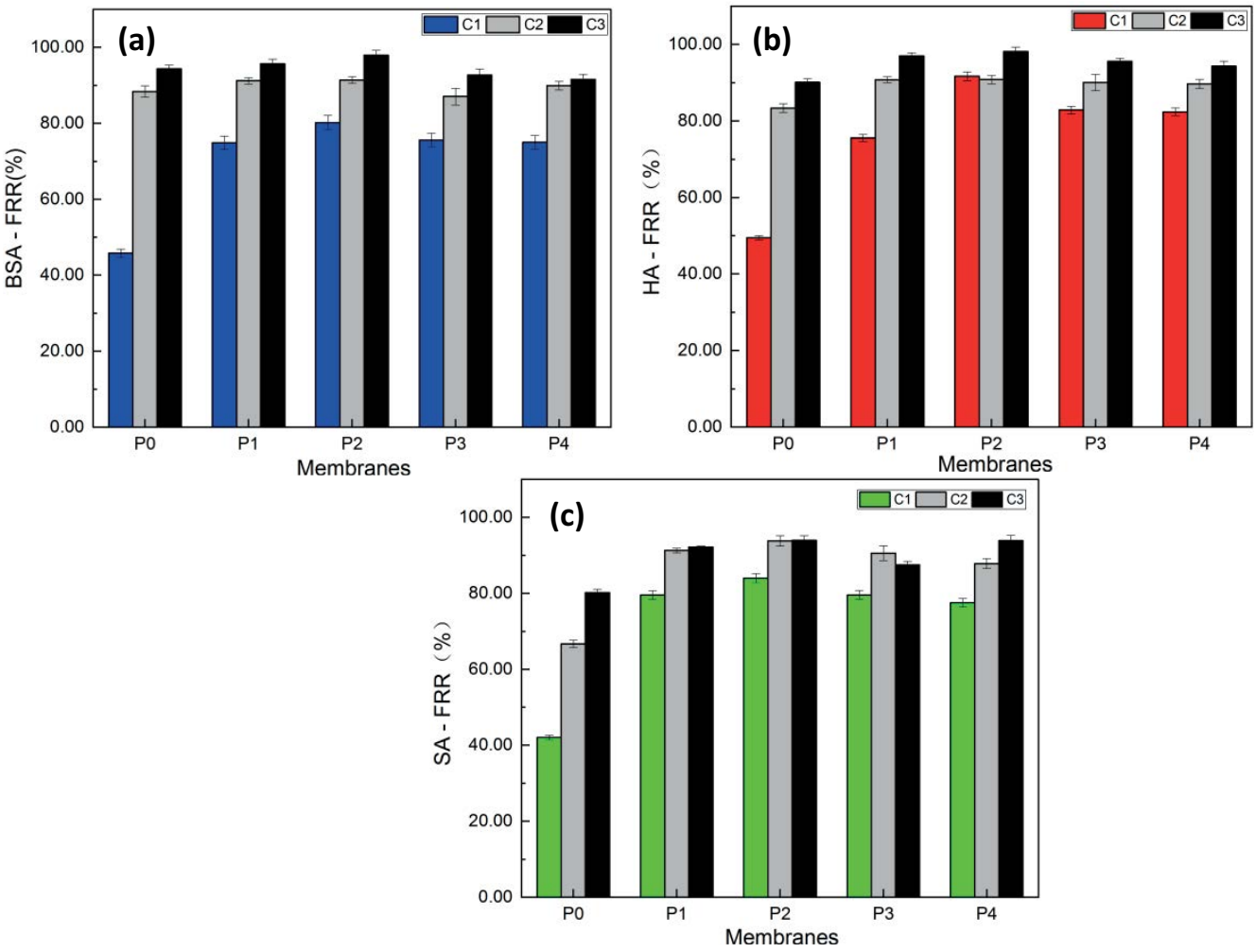

Fig. 13. Flux recovery rate of modified polysulfone membrane in three cycles: (a) BSA, (b) HA and (c) SA.

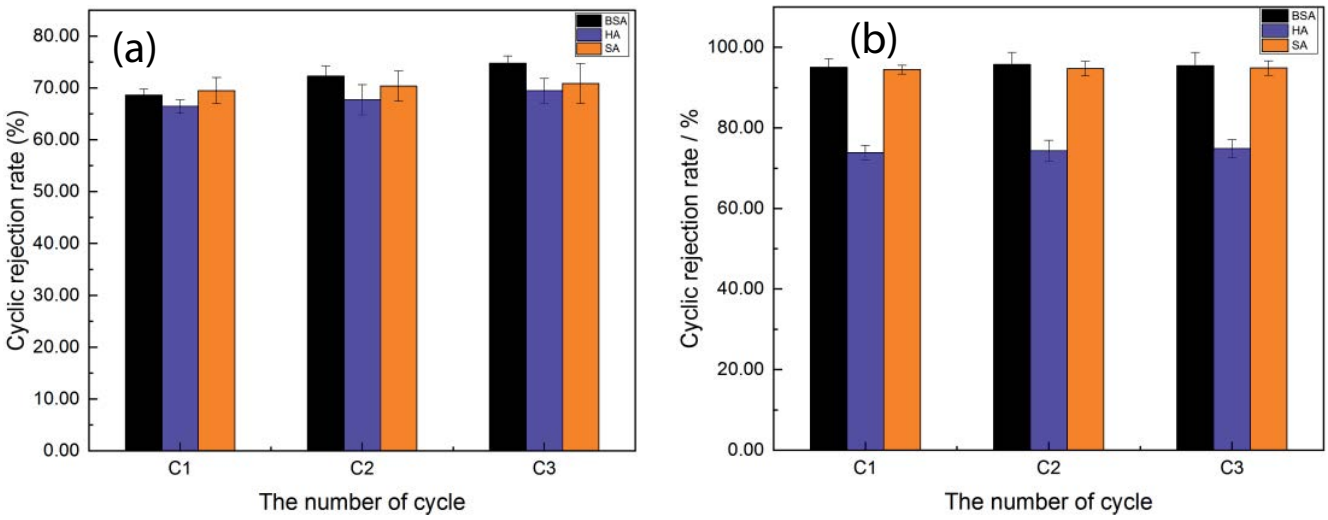

Fig. 14. Interception rate of three circulating pollutants: (a) P0 and (b) P2.

channels during filtration. After backwashing, some pollutants fall off washing and the flux rises. After three cycles, the flux recovery of the modified membrane is significantly higher than that of the original membrane, indicating that the introduction of $ZnFe_2O_4$-rGO particles improves the cycling performance of the ultrafiltration membrane.

The composite membrane flux recovery results after three pollution cycles are shown in Fig. 13. The results showed that $ZnFe_2O_4$-rGO films with a loading capacity of 0.04 wt.% had the best resistance to contamination, and the maximum flux recovery of BSA, HA and SA reached 97.92%, 98.15% and 93.95%, respectively. In addition, in Fig. 14 the rejection rates of BSA and SA in P0 film were 68.60%, 72.31%, 74.80% and 69.50%, 70.37%, 70.89% after three cycle. While, the rejection rates of BSA and SA of P2 (0.04 wt.%) were 95.03%, 95.74%, 95.46% and 94.50%, 94.72%, 94.87%. Combined with the recovery of circulating flux, the results showed that the membrane pore "collapsed" after three times of pollution, and the blockage of pollutants blocked the membrane permeability and showed an enhanced interception effect. However, the modified membrane showed a relatively stable interception effect, indicating that the modified membrane still maintained a relatively stable pollutant interception effect after three times of pollution.

4. Conclusion

In this work, $ZnFe_2O_4$-rGO/PSF composite films were prepared by immersion precipitation phase transformation method. The water contact angle decreased from 88.2° to 63.5°, the pure water flux increased from 230.24 to 517.06 LMH·bar^{-1}, the membrane resistance decreased from 2.62×10^{12} m^{-1} to 1.17×10^{12} m^{-1}. The stability of casting solution was obviously improved pore-forming ability, which led to the thickness of the top layer was reduced. After that, the higher porosity resulted in the hydrophilicity and permeability enhancement of the UF. The results of interception and anti-fouling analysis showed that the optimal loading capacity of the particle was 0.04 wt.%, and the rejection rates of BSA, HA, and SA were 95.03%, 73.89% and 94.50%, respectively. The irreversible pollution was decreased to 19.80%, 19.98% and 15.98%. Besides, the strength increased by 85.28 cN and the elongation increased by 10.22% with the addition of particles. After three cycles, the rejection rates were kept 94.50%, 94.72%, 94.87%. The maximum flux recovery was 97.92%, 98.15%, and 93.95%. The results showed that appropriate doping of particles not only improved the separation and interception of polysulfone membrane but also significantly alleviated the membrane fouling caused by pollutant blocking. The results of flux change, flux recovery and pollutant interception showed that the prepared composite membrane could maintain relatively stable permeability and interception effect after several cycles, which significantly improved the poor permeability of the neat membrane, the rapid collapse of membrane pores after contamination, and poor circulation practicability.

Acknowledgement

The financial supports from the Natural science research project of Anhui Provincial Department of Education (KJ2020A0078) were acknowledged.

References

[1] Y.Y. Tang, J. Xu, C.J. Gao, Ultrafiltration membranes with ultrafast water transport tuned via different substrates, Chem. Eng. J., 303 (2016) 322–330.
[2] C.Y. Yang, Q. Wang, G.S. Zhang, P. Wang, Preparation and catalytic performance of photocatalytic composite ultrafiltration membrane, Chin. Environ. Sci. J., 37 (2017) 4564–4570.
[3] M.Y. Hu, Z.Y. Cui, J. Li, L. Zhang, Y.H. Mo, D.S. Dlamini, H. Wang, B.Q. He, J.X. Li, H. Matsuyama, Ultra-low graphene oxide loading for water permeability, antifouling and antibacterial improvement of polyethersulfone/sulfonated polysulfone ultrafiltration membranes, J. Colloid Interface Sci., 552 (2019) 319–331.
[4] S.B. Liu, Z. Wang, P. Song, Free radical graft copolymerization strategy to prepare catechin-modified chitosan loose nanofiltration (NF) membrane for dye desalination, ACS Sustainable Chem. Eng., 6 (2018) 4253–4263.
[5] A. Abedalkader, Q. Hazim, Novel polysulfone ultrafiltration membranes incorporating polydopamine functionalized graphene oxide with enhanced flux and fouling resistance, J. Membr. Sci., 620 (2021) 118900, doi: 10.1016/j.memsci.2020.118900.
[6] L.F. Zhu, M.Y. Wu, B. Van der Bruggen, L.C. Lei, L.Z. Zhu, Effect of TiO_2 content on the properties of polysulfone nanofiltration membranes modified with a layer of TiO_2–graphene oxide, Sep. Purif. Technol., 242 (2020) 116770, doi: 10.1016/j.seppur.2020.116770.
[7] X.J. Li, A. Janke, P. Formanek, A. Fery, M. Stamm, B.P. Tripathi, High permeation and antifouling polysulfone ultrafiltration membranes with *in situ* synthesized silica nanoparticles, Mater. Today Commun., 22 (2019) 100784, doi: 10.1016/j.mtcomm.2019.100784.
[8] H.Q. Wu, Y.J. Liu, J. Huang, L. Mao, J.H. Chen, M. Li, Preparation and characterization of antifouling and antibacterial polysulfone ultrafiltration membranes incorporated with a silver–polydopamine nanohybrid, J. Appl. Polym. Sci., 135 (2018) 46430, doi: 10.1002/app.46430.
[9] Y.K. Kim, D. Rana, T. Matsuura, W.-J. Chung, K. Khulbe, Relationship between surface structure and separation performance of poly(ether sulfone) ultra-filtration membranes blended with surface modifying macromolecules, Sep. Purif. Technol., 72 (2010) 123–132.
[10] D. Rana, T. Matsuura, R.M. Narbaitz, C. Feng, Development and characterization of novel hydrophilic surface modifying macromolecule for polymeric membranes, J. Membr. Sci., 249 (2005) 103–112.
[11] D. Rana, T. Matsuura, R.M. Narbaitz, Novel hydrophilic surface modifying macromolecules for polymeric membranes: polyurethane ends capped by hydroxy group, J. Membr. Sci., 282 (2006) 205–216.
[12] D. Rana, R.M. Narbaitz, A.-M. Garand-Sheridan, A. Westgate, T. Matsuura, S. Tabe, S.Y. Jasim, Development of novel charged surface modifying macromolecule blended PES membranes to remove EDCs and PPCPs from drinking water sources, J. Mater. Chem. A, 2 (2014) 10059–10072.
[13] Y.K. Kim, D. Rana, T. Matsuura, W.-J. Chung, Towards antibiofouling ultrafiltration membranes by blending silver containing surface modifying macromolecules, Chem. Commun., 48 (2012) 693–695.
[14] C.Y. Yu, Controlled Synthesis and Photocatalytic Properties of Graphene-Carbon Nitride Zinc Ferrite Composites, Nanjing University of Science and Technology, China, 2018.
[15] T. Etemadinia, B. Barikbin, A. Allahresani, Removal of Congo red dye from aqueous solutions using $ZnFe_2O_4$/SiO_2/Tragacanth gum magnetic nanocomposite as a novel adsorbent, Surf. Interfaces, 14 (2019) 117–126.
[16] A. Hussein Mady, M. Lara Baynosa, D. Tuma, J.-J. Shim, Facile microwave-assisted green synthesis of Ag-$ZnFe_2O_4$@rGO nanocomposites for efficient removal of organic dyes under UV- and visible-light irradiation, Appl. Catal., B, 203 (2017) 416–427.
[17] R.R. Lan, Preparation and Properties of Rare Earth Modified Barium Ferrite/PVDF Composite Films, Shanghai Normal University, China, 2020.

[18] P. Kallem, I. Othman, M. Ouda, S.W. Hasan, I. AlNashef, F. Banat, Polyethersulfone hybrid ultrafiltration membranes fabricated with polydopamine modified $ZnFe_2O_4$ nanocomposites: applications in humic acid removal and oil/water emulsion separation, Process Saf. Environ. Prot., 148 (2021) 813–824.
[19] D. Rana, K. Bag, S.N. Bhattacharyya, B.M. Mandal, Miscibility of poly(styrene-*co*-butyl acrylate) with poly(ethyl methacrylate): existence of Both UCST and LCST, J. Polym. Sci., Part B: Polym. Phys., 38 (2000) 369–375.
[20] W. Ding, L.J.H. Huang, W. Huang, X. Zhang, Research progress of modified organic nanofiltration membrane, Mod. Chem. Ind., 40 (2020) 21–24, 29 (in Chinese).
[21] W.Q. Jin, Graphene nanoscreen/carbon nanotube nanofiltration membrane, Acta Phys. Chim. Sin., 35 (2019) 1301–1302 (in Chinese).
[22] X.M. Hu, W.X. Yang, T. Li, Preparation and filtration performance of GO/polyvinylidene fluoride composite fiber filter membrane, Text. Res. J., 40 (2019) 32–37.
[23] H.D. Zhang, J.W. Chen, L.C. Zhang, J. Chen, Preparation of hydrophobic oil-philic film based on reduced graphene oxide and its application in oil-water separation, New Chem. Mater., 47 (2019) 223–227 (in Chinese).
[24] K. Wu, Preparation and Properties of Magnetic $ZnFe_2O_4$ Composite Photocatalytic Materials, Zhejiang University of Technology, China, 2019.
[25] L. Shen, J.H. Pan, R. Jiang, L. Hu, Photocatalytic decoloration of dye wastewater by $ZnFe_2O_4$/graphene nanosheet composites, Text. Print. Dying Additive, 32 (2015) 29–32 (in Chinese).
[26] X.S. Zhang, Preparation and Properties of Hydrophilic Polysulfone Ultrafiltration Membrane, Changchun University of Technology, China, 2020.
[27] R. Singh, M.K. Sinha, M.K. Purkait, Stimuli responsive mixed matrix polysulfone ultrafiltration membrane for humic acid and photocatalytic dye removal applications, Sep. Purif. Technol., 250 (2020) 117247, doi: 10.1016/j.seppur.2020.117247.
[28] Y.H. Zhang, Study on Porous Graphene Oxide Modified Ultrafiltration Membrane and Its Removal Efficiency for Natural Organic Matter, Harbin Institute of Technology, China, 2020.
[29] J.T. Feng, Y.C. Wang, Y.H. Hou, L.C. Li, Hierarchical structured $ZnFe_2O_4$@rGO@TiO_2 composite as powerful visible light catalyst for degradation of fulvic acid, J. Nanopart. Res., 19 (2017) 178, doi: 10.1007/s11051-017-3842-6.
[30] N. Nasrollahi, S. Aber, V. Vatanpour, N.M. Mahmoodi, Development of hydrophilic microporous PES ultrafiltration membrane containing CuO nanoparticles with improved antifouling and separation performance, Mater. Chem. Phys., 222 (2019) 338–350.